THE JOURNAL OF PHYSICAL CHEMISTRY C

Article

pubs.acs.org/JPCC

Biphasic Resistive Pulses and Ion Concentration Modulation during Particle Translocation through Cylindrical Nanopores

Kaikai Chen,[†] Lei Shan,[†] Siyuan He,[‡] Guoqing Hu,[‡] Yonggang Meng,[†] and Yu Tian*[,†]

[†]State Key Laboratory of Tribology, Tsinghua University, Beijing 100084, China

[‡]Institute of Mechanics, Chinese Academy of Sciences, Beijing 100190, China

Supporting Information

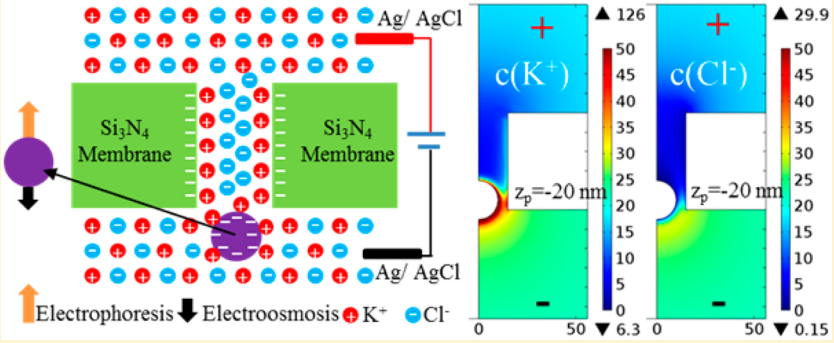

ABSTRACT: We investigated the biphasic resistive pulses during particle translocation through cylindrical nanopores at low salt concentration by simulation, and the effects of electrolyte concentration, surface charge, electric potential, and pore geometry were systematically discussed. The formation of positive peaks in the pulses is ascribed to the surface charge on the particle and the pore. The peak current enhancement/decline ratio increases linearly with the particle surface charge density but decreases with the salt concentration increase. We find that there is an optimum electric potential for the peak current enhancement ratio to reach the maximum value. When a negatively charged particle is at the orifice of the pore on the low/high potential side, the ion concentration inside and around the pore is significantly depleted/enriched, while inverse electric potential or inverse surface charge has an opposite effect. The extent of such ion modulation is larger with a longer pore. The peak current enhancement/decline ratio is quantitatively linked to the percent of ion concentration enrichment/depletion inside and around the pore, by considering particle occupied volume and concentration change.

I. INTRODUCTION

Solid-state nanopores are emerging as promising tools for detecting biomolecules or nanoparticles by analyzing resistive pulses during their translocation through the pores.[1−7] The basic principle of nanopore detection originates from the Coulter counter,[8] where particles inside a micro tube occupy the electrolyte volume and hence decrease the pore conductance. Translocation of biomolecules and nanoscale materials with a wide range of size and geometry has been reported.[9−11] While one of the fascinating goals of nanopore detection may be the next generation DNA sequencing, its potential application in characterizing nanoparticle surface charge and size has been also widely discussed.[12−15] Submicrometer particles and biological molecules were detected by polymer pores by DeBlois, Wesley, etc. in 1970s.[16,17] Recently, silicon nitride nanopores and glass conical nanopores are used for particle detection with the translocation of polystyrene particles, silica particles and gold nanoparticles.[18−22]

In most cases, negative resistive pulses are observed since particles block the ionic current. However, positive peaks and unexpected waveshapes were reported for DNA translocation at low electrolyte concentration,[22−29] and were recently shown during particle or PEG translocation.[30−34] The translocation of cylindrical particles was reported with a biphasic pulse at salt concentration 0.01 M and the electrokinetic motion was shown by simulation.[35,36] The cation and anion distributions were also shown in ref 35 where they are not equal to the bulk concentration. Goyal (2013) investigated gold nanoparticle translocation using silicon nitride nanopores and observed ionic current enhancement upon particle translocation in 20 mM KCl solution.[30] Menestrina (2014) and Innes (2014) reported positive peaks following negative pulses when charged polystyrene particles translocated through micro size polyethylene terephthalate pores.[31,32] Biphasic pulses were also reported during particle translocation through glass conical nanopores (Lan, 2014).[33] Unusual current blockade induced by oxidized PEG translocation was reported with current decrease/increase when the PEG was at the entrance/exit (Cabello-Aguilar, 2014).[34] In the experiments, the biphasic

Received: January 3, 2015
Revised: March 23, 2015
Published: March 30, 2015

DOI: 10.1021/acs.jpcc.5b00047
J. Phys. Chem. C 2015, 119, 8329−8335

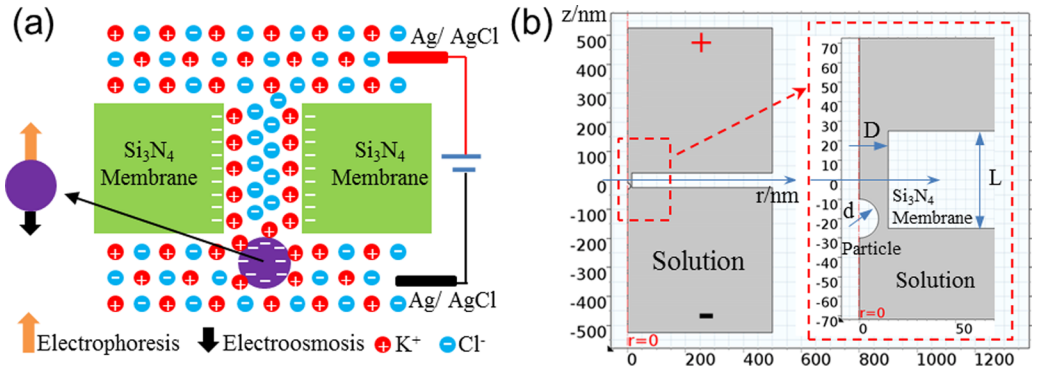

Figure 1. Schematic (a) and the simulation model (b) of a negatively charged particle translocation through a negatively charged cylindrical nanopore in a KCl solution. L = 50 nm, D = 30 nm, and d = 20 nm are used in the simulation unless otherwise specified.

resistive pulses only exited with low salt concentration and high voltage.[28,33] and in some experiment even only current enhancement was observed.[30] The positive standard bias (the ratio of current enhancement/decrease to base current) increased while the negative standard bias decreased with the voltage increase in Goyal's experimetn.[30]

Those unexpected resistive pulses are interesting subjects to be investigated to understand the basic principles of particle translocation through nanaopores. Some researchers considered that the current enhancement was due to counterions around the particles when the particle size and pore size were comparable to the thickness of the electric double layer (EDL). The phenomenon was also demonstrated in experiments with micro size pores, and Menestrina proposed that the formation of positive peaks was due to the ion concentration modulation but did not give a quantitative link.[31] When the system size increases from nanometer to micrometer, the effect of EDL may become smaller. However, the effect should be finally determined by the gap distance between the pore and particle rather than the overall size, since it is the gap distance that influences the behaviors of the ions and the fluid. Lan compared the experimental results and simulation results with conical glass nanopores,[33] however, for small cylindrical nanopores, the biphasic resistive pulses are to be studied in detail.

In this study, we used numerical simulation to analyze the current waveshape and ion concentration. The modeling method is similar to that in ref 33, while we show a more detailed discussion on the resistive pulses with cylindrical nanopores, considering the combined effects of electrolyte concentration, surface charge, electric potential and pore geometry. Since the transition from current-position curves to current−time curves did not change the current magnitude on the vertical axis,[20] we obtained the current-position curve as a reflection of the recorded signal in time. The direction of translocation is determined by the surface charge and electric field. Theoretically, when the particle surface charge is larger/smaller than the pore surface charge, the particle moves in the direction of electrophoresis/electroosmosis.[9,22] The directions of particle motion in the current-position traces are shown by arrows. Negative or positive surface charge was applied on the particles and pores with different applied potentials. The current-position traces are demonstrated, and we quantitatively verified the link between the current peaks of the resistive pulses to the ion concentration modulation extent.

II. MODEL AND METHODS

Figure 1a shows the schematic of a negatively charged particle translocation through a negatively charged pore. Axially symmetric geometry was used in the model, as shown in Figure 1b, where D, L, d, and z_p are the pore diameter, pore length, particle diameter, and particle position respectively (z_p = 0 at the middle of the pore length). To achieve accurate results, the mesh resolution is high enough and the reservoir size in the model was increased to ensure that no change in calculated current and ion concentration was observed.[37] The particle is assumed to translocate through the pore along the symmetric axis, and thus the influence of particle deviation from the axis on the ionic current is neglected. Poisson−Nernst−Planck (PNP) equations and the Navier−Stokes (NS) equation were coupled to solve the ionic current and ion concentration with the commercial software Comsol Multiphysics.

The potential distribution can be expressed by the Poisson equation,

$$\nabla^2 E = -\frac{\rho}{\varepsilon_r \varepsilon_0} = -\frac{F}{\varepsilon_r \varepsilon_0} \sum_i z_i c_i \tag{1}$$

where E, ρ, ε_r, ε_0, F, z_i, c_i are the electric potential, electric charge density, relative permittivity, dielectric constant, Faraday constant, ion valence and ion molar concentration, respectively. The Nernst−Planck equation

$$\vec{\nabla}\cdot(-D_i\vec{\nabla}c_i - z_i\mu_i c_i\vec{\nabla}E) = -\vec{u}\cdot\vec{\nabla}c_i \tag{2}$$

is a continuity equation, where D_i is the diffusion coefficient, μ_i is the ion mobility and $\vec{u}$ is the fluid velocity. The Navier−Stokes equation is

$$\eta\nabla^2\vec{u} - \vec{\nabla}p - F\sum_i z_i c_i(r)\vec{\nabla}E = 0 \tag{3}$$

In the equation, η and p denote fluid viscosity and pressure, respectively.

As shown in Figure 1b, the lower boundary of the reservoir is grounded and the electric potential is applied on the upper boundary. The ionic current was calculated when the particle was at a series of positions along the symmetric axis to obtain the current-position trace. First, 20 mM KCl solution was used as the electrolyte at electric potential 1 V. The pore length L, pore diameter D, and particle diameter d were set to be 50, 30, and 20 nm respectively unless otherwise specified, similar to the experimental condition in ref 30. Then the particle surface charge density σ_{pa}, pore surface charge density σ_{po}, KCl

DOI: 10.1021/acs.jpcc.5b00047
J. Phys. Chem. C 2015, 119, 8329−8335

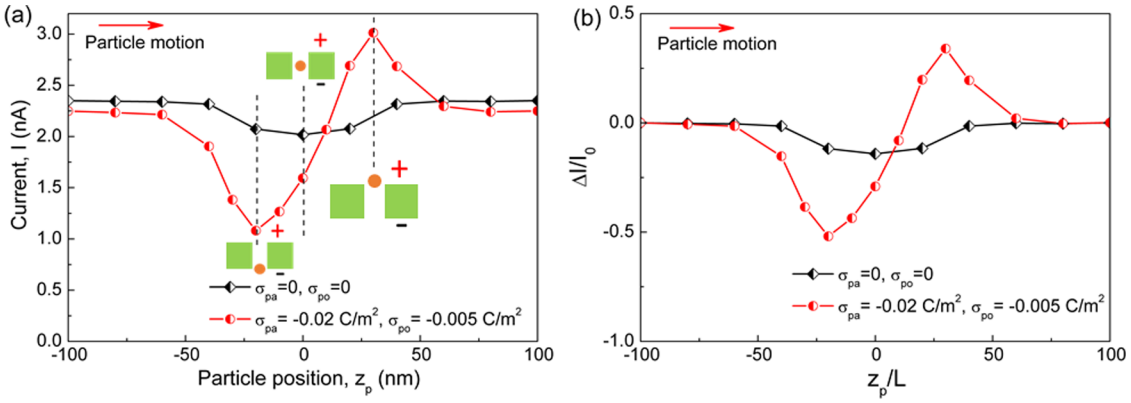

Figure 2. Formation of biphasic resistive pulse in current-position trace (a) and normalized current deviation (ratios of current deviation ΔI to the base current I_0) (b) with surface charge density σ_{pa}=-0.02 C/m^2 and σ_{po} = −0.005 C/m^2 in 20 mM KCl solution. The electric potential is 1 V.

concentration, electric potential, and pore geometry were changed to show the current waveshape and ion concentration distribution in different cases.

III. RESULTS AND DISCUSSION

Biphasic Resistive Pulse and Peak Current Deviation. We analyzed particle translocation without the effect of surface charge as a reference (Figure 2a) although this case rarely exists in experiments. In most cases, particles and pores are negatively charged with solution pH > 7. The pore surface can be modified by atomic layer deposition to obtain uncharged characters, and this can influence the mobility and the energy barrier.[38] When typical surface charge (particle −0.02 C/m^2, pore −0.005 C/m^2) was applied,[33] a biphasic pulse was observed, which was reported in former experiments with cylindrical micropores and conical nanopores.[31−33] Obviously, the waveshape and base current are changed by the surface charge, and the normalized peak current deviations (ratios of peak current deviations from the base current to the base current) are much larger than those without surface charge. Notably, the normalized negative peak deviation and positive peak deviation are 52% and 34% respectively, larger than the value of 14% without surface charge (Figure 2b). Therefore, the surface charge of the particle improves the signal-to-noise ratio at low salt concentration.

In the above case, both the pore and particle are charged. Menestrina's experiment shows that the positive peak was caused by the particle surface charge but not the pore surface charge.[31] To study their effects separately, translocations of uncharged particles through charged pores and charged particles through uncharged pores were investigated. As shown in Figure 3a, the effect of pore surface charge (−0.005 C/m^2) is slight compared to the effect of particle surface charge (−0.02 C/m^2). When the pore carries a larger surface charge (−0.02 C/m^2), the base current decreases significantly and there is also a biphasic pulse. This was not reported in Menestrina's experiment and it may be due to the low pore surface charge or the large geometry used by them. In our simulation, both the particle surface charge and pore surface charge induce biphasic pulses. The negative peak and positive peak occur near the particle positions z_p= −20 nm and z_p = 30 nm, respectively. It should be noted that they are not the symmetric positions at z_p= −25 nm and z_p= 25 nm when half of the particle was in the pore, and the current waveshape is not symmetric as well.

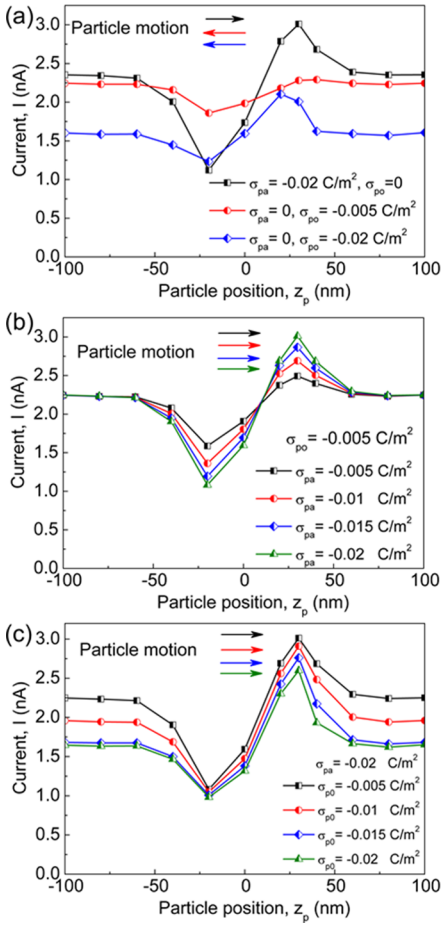

Figure 3. Effects of surface charge density on current waveshape. (a) Effects of particle surface charge and pore surface charge, respectively. (b) Effect of particle surface charge density with σ_{po} = −0.005 C/m^2. (c) Effect of pore surface charge density with σ_{pa} = −0.02 C/m^2. A 20 mM KCl solution and 1 V electric potential are used in the simulation.

To explore the combined effects of surface charge, we changed the pore surface charge and particle surface charge respectively, and the current-position traces are shown in Figure 3, parts b and Figure c. The magnitude of particle surface charge does not influence the base current, but has a significant effect on the peak current deviation. With a constant pore surface charge −0.005 C/m^2, both the normalized positive peak deviation and normalized negative peak deviation increase

DOI: 10.1021/acs.jpcc.5b00047
J. Phys. Chem. C 2015, 119, 8329−8335

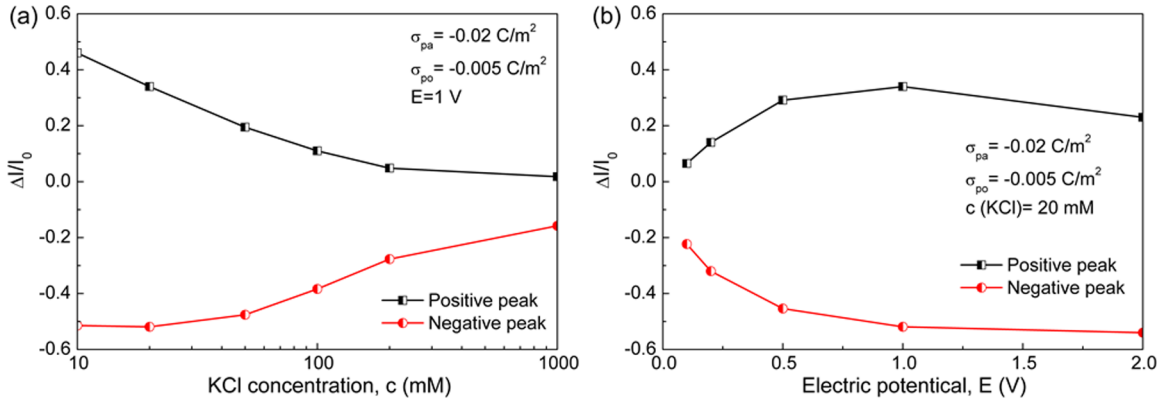

Figure 4. Effect of KCl concentration at electric potential 1 V (a) and the effect of electric potential in 20 mM KCl solution (b) on normalized current peak values. σ_{pa} = −0.02 C/m^2 and σ_{po} = −0.005 C/m^2 are used in the simulation.

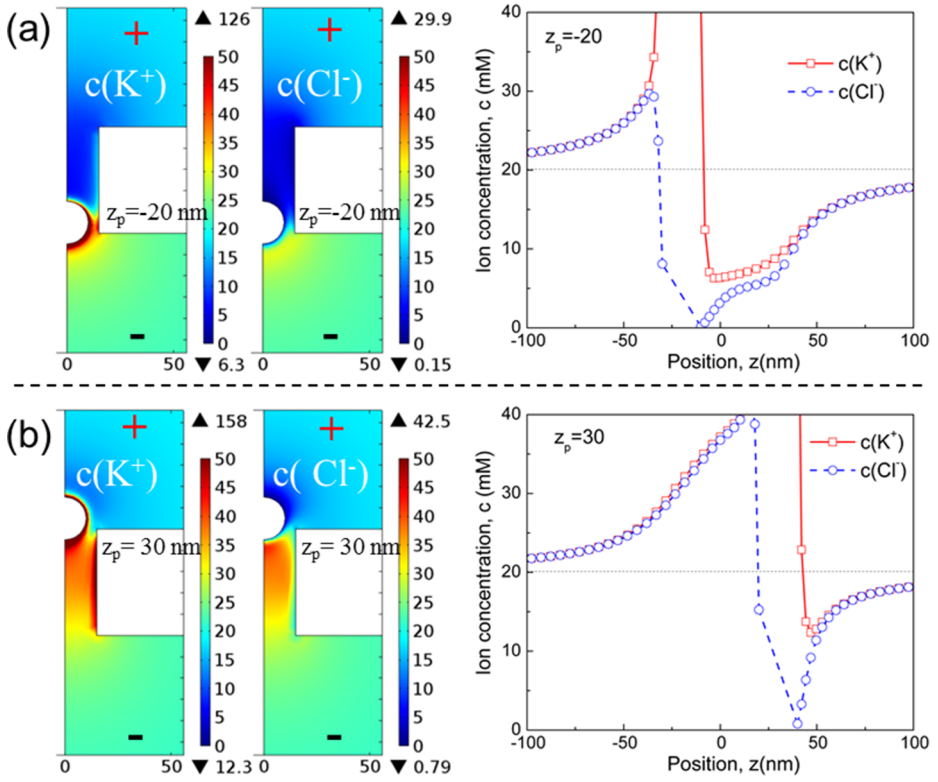

Figure 5. Concentration distribution of K^+ and Cl^- at particle position z_p = −20 (a) and z_p = 30 (b) in 20 mM KCl solution. σ_{pa} = −0.02 C/m^2, σ_{po} = −0.005 C/m^2 and E = 1 V are used in the simulation. The right panels show the ion concentration along the axis.

linearly with the particle surface charge density (Figure S1(a), Supporting Information). The magnitude of pore surface charge changes both the base current and the peak current deviation. With a constant particle surface charge −0.02 C/m^2 and the increase of pore surface charge, the base current decreases while the normalized positive and negative peak deviations do not increase and decrease monotonously (Figure S1(b)).

When the particle and the pore are positively charged, the positive peak current and negative peak current occur at particle positions around z_p = −30 nm and z_p = 20 nm, respectively. In this case, the particle would move along the direction with the decrease of z_p, and the current−time trace would be similar to that during a negatively charged particle translocation through a negatively charged pore.

In previous experiments, the biphasic pulse only existed at low salt concentration with a high biased voltage.[30−33] With the same geometry and surface charge magnitude, salt concentration and applied electric potential were varied to explore their effects on current waveshape. Figure 4a shows both the normalized positive and negative peak current deviations decreased with the increase of KCl concentration from 10 mM to 1 M. As expected, the positive peaks are observed when the salt concentration was smaller than 100 mM, but the peak value disappears gradually when the concentration is larger than 200 mM. Figure 4b shows that there is an optimum voltage between 0 and 2 V for the normalized positive peak current deviation to reach its maximum value. However, we did not find corresponding experimental results in the references dealing with biphasic pulses and this can be further studied.[22−34] The negative peak value becomes larger as the electric potential

DOI: 10.1021/acs.jpcc.5b00047
J. Phys. Chem. C 2015, 119, 8329−8335

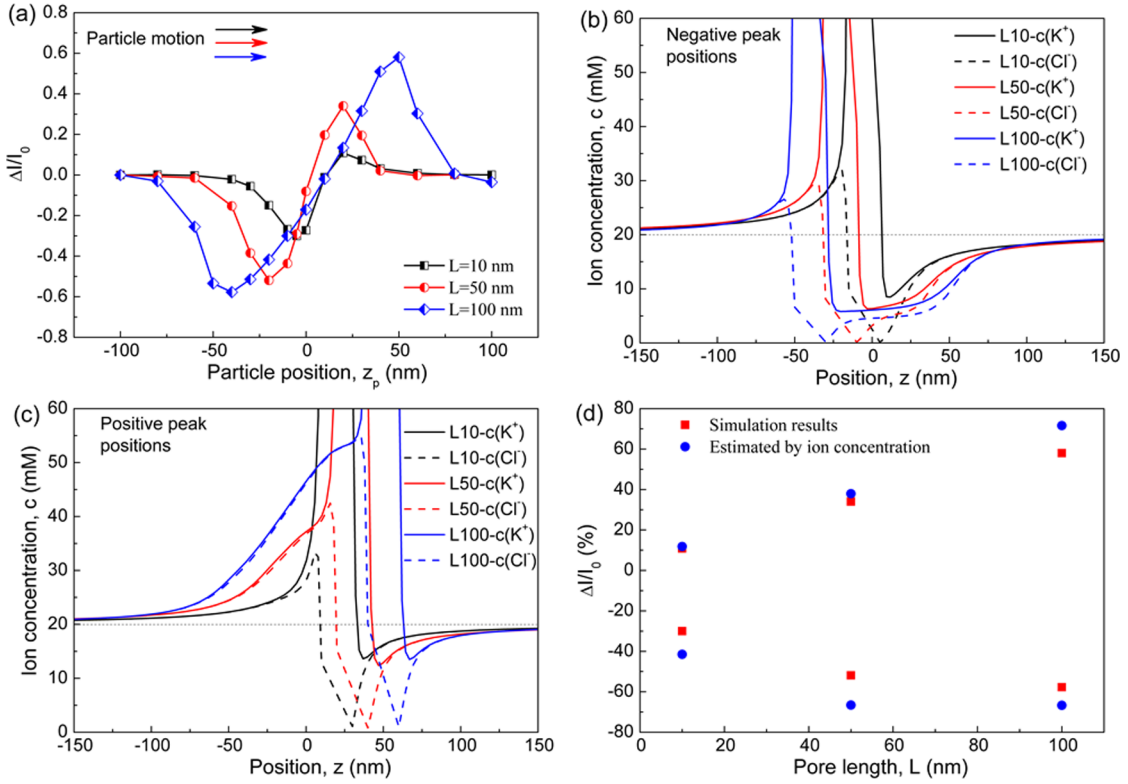

Figure 6. Current waveshape and ion concentration modulation with different pore length at 1 V in 20 mM KCl solution. (a) Current waveshape. (b) Ion concentration distribution along the axis when the particle was at the negative current peak positions. (c) Ion concentration distribution along the axis when the particle was at the positive current peak positions. (d) Comparison between the estimated values by concentration and simulation results. D = 30 nm, d = 20 nm, σ_{pa} = −0.02 C/m^2 and σ_{po} = −0.005 C/m^2 are used in the simulation.

increases and is saturated at electric potentials larger than 1 V. However, if the electric field is inversed, the positive peak and the negative peak occur near particle positions z_p = −30 nm and z_p = 20 nm respectively (Figure S2). It should be noted that with the inverse electric field, the particle motion direction is changed, so the current curves in time may be similar.

Ion Concentration Modulation. Menestrina reported that the current decrease/increase was due to ion concentration modulation.[30] We investigated the ion concentration distribution at the particle positions with positive and negative peak current in Figure 2. Parts a and b of Figure 5 show the cation and anion distribution at the two particle positions (z_p=-20 nm and z_p = 30 nm). The right panels show the ion concentration along the axis. The ion concentration decreases on the side of the particle with higher potential while increases on the side with lower potential. This phenomenon is similar to that in current rectification, which was reported in experiments with asymmetric pore geometry, asymmetric surface charge or the combination of them.[39] When the particle is at the position z_p = −20 nm (Figure 5a), the gap between the particle and the pore serves as a gate with a cation-selective function. K^+ ions in the pore move to the low potential side driven by the electric field while the transport of Cl^- ions from the low potential side into the pore is rejected by the gate. The consequence is the ion concentration decrease in the pore. On the other hand, at the particle position z_p = 30 nm (Figure 5b), K^+ ions flow into the pore while the motion of Cl^- ions out of the pore is rejected, causing an increases of ion concentration in the pore. The phenomenon is more significant when the electric double layers overlapped. The maximum modulation does not happen at positions z_p = ± 25 nm when the gap distance is smaller and closer to the sum of the Debye length. We do not have a good explanation on the positions of the negative and positive peaks, and we assume that it is ascribed to the complex combined effect of the electric field and surface charge.

When the particle and the pore are positively charged, the gap is anion-selective, so Cl^- flux into the pore is promoted and K^- flux out of the pore is rejected at particle position z_p = −20 nm. Therefore, the effect on ion modulation is inversed (Figure S3). Similarly, with a negative electric potential the modulation effect inside the pore is also inversed (Figure S4).

Linking the Peak Current Deviation to Ion Concentration Change. With constant electric potential, the ionic current is determined by the pore resistance R_p and the access resistance R_a, and they can be approximately calculated as[40,41]

$$R_p = \frac{1}{\kappa}\int_{-L/2}^{L/2}\frac{1}{A(z)}\,dz \tag{4}$$

$$R_a = \frac{1}{\kappa D} \tag{5}$$

In the equations, κ is the electrical conductivity of the electrolyte. However, if the ion concentration in the pore is not equal to the bulk concentration, the pore conductance would be determined by the ion concentration distribution.

Without the effect of the particle, the resistance of the open pore is then $R_{po} = ((4L)/(\kappa_{bulk}\pi D^2))$, where κ_{bulk} is the conductance of the bulk solution. The ratio of open access resistance R_{ao} to open pore resistance R_{po} is

$$\alpha = \frac{\pi D}{4L} \approx 0.8\frac{D}{L} \tag{6}$$

DOI: 10.1021/acs.jpcc.5b00047
J. Phys. Chem. C 2015, 119, 8329−8335

The open access resistance on each side is $R_{ao1} = R_{ao2} = 0.5R_{ao} \approx 0.4R_{po}D/L$.

When the charged particle is at the orifice, supposing the ratio of particle volume in the pore to the pore volume is λ, from eq 4, the blocked pore resistance is $R_{pb} = ((\kappa_{bulk})/(\kappa_{ave}))(1/(1-\lambda))R_{po}$, where κ_{ave} is the average conductivity of the solution in the pore. Assuming that the salt conductivity has a linear relationship with ion concentration, the blocked pore resistance is

$$R_{pb} = \frac{c_{bulk}}{c_{ave}} \frac{1}{1-\lambda} R_p \tag{7}$$

where c_{bulk}, c_{ave} are the bulk ion concentration and average ion concentration in the pore. Neglecting the effect of particle on access resistance, the blocked access resistance R_{ab1} and R_{ab2} can be determined by the following equations:

$$R_{ab1} = \frac{c_{bulk}}{c_{en}} R_{ao1} \tag{8}$$

$$R_{ab2} = \frac{c_{bulk}}{c_{ex}} R_{ao2} \tag{9}$$

In the equations, c_{en} and c_{ex} denote the ion concentration at the entrance and ion concentration at the exit, respectively. So the current drop or enhancement ratio is

$$\frac{\Delta I}{I_0} = \frac{R_{po} + R_{ao1} + R_{ao2}}{R_{pb} + R_{ab1} + R_{ab2}} - 1 \tag{10}$$

We used eq 10 to calculate the peak values, and obtained the normalized negative and positive peak deviations 66.6% and 37.9% respectively in the case in Figure 2a. The large error (66.6% vs 52%) for negative value is due to the uneven ion concentration distribution around the particle. The neglected particle effect on access resistance also contributed to the error.[37] However, the results showed the negative and positive peaks could be similarly estimated by the change of ion concentration. The standard deviation values in ref 30 are between 0.4 and 0.74 with voltage 100−400 mV. The values are influenced by the surface charge and voltage simultaneously, and the factors should be tuned to match the experimental results.

As shown in Figure 6a, with the increase of pore length from 10 to 100 nm (corresponding to D/L from 3 to 0.3), the normalized peak current deviation increases. It is due to the larger ion concentration depletion/enhancement effect for longer pores when the particle is at the entrance/exit as shown in Figure 6, parts b and Figure c. The peak values are estimated using the above method and are compared to the simulation results, as shown in Figure 6d. The estimated positive peak value for 10 nm long pore is closer to the calculated values since the particle is not in the pore when the current has the peak value, and the effect of the particle occupied volume on current change is small enough compared to the effect of ion concentration modulation. In other cases, the peak current occurs when a part of the particle or the whole particle is in the pore, making the ion concentration unevenly distributed around the pore, and the error and relative error are larger compared with those for positive peak value with 10 nm long pore.

Low concentration KCl solutions are often used in nanoparticle detection to avoid particle aggregation. The above results show the origin of the current enhancement and biphasic pulse induced by surface charge during particle translocation through nanopores. However, in ref 30, the experimental results show only current enhancement which could not be explained by our simulation and Menestrina's simulation in ref 31. So we still do not have a good explanation for the results in ref 30, and we assumed that it was caused by the particle motion. The assumption of immobile particle in the simulation neglects the effect of particle diffusion, electrophoretic and electro-osmotic motion on the ionic current. Hopefully, it explains the formation of biphasic pulses by demonstrating the ion concentration in details and shows the redistribution of ions induced by surface charge and electric potential, yet a more precise simulation considering the complex particle motion and more experiments are needed to fully understand the phenomenon.

IV. CONCLUSIONS

In this article, we analyze the biphasic resistive pulses and ion concentration distribution during particle translocation through nanopores in low concentration electrolyte. The normalized positive peak current deviation is large at a low salt concentration, high particle surface charge and a moderate electric potential. The ion concentration is enhanced or depleted when the particle was at the pore orifice induced by surface charge and electric field. The inverse electric field or surface charge has an opposite effect on ion concentration distribution inside the pore. The peak current deviation of the biphasic pulse is quantitatively linked to the ion concentration modulation. Understanding the principle of surface charge and electric field induced ion concentration are helpful in interpreting nanopaticle translocation though nanopores and in choosing appropriate experimental conditions. Furthermore, it is helpful in analyzing particle surface charge, improving signal-to-noise ratio, and determining the translocation direction by analyzing the resistive pulse.

■ ASSOCIATED CONTENT

Supporting Information

Figures showing results on effects of particle surface charge and pore surface charge on normalized peak current deviation and effect of inversed electric field on current waveshape and ion concentration distribution with inversed surface charge and with inversed electric potential. This material is available free of charge via the Internet at http://pubs.acs.org.

■ AUTHOR INFORMATION

Corresponding Author

*(Y.T.) Telephone: (+86) 010 62782981. E-mail: tianyu@mail.tsinghua.edu.cn.

Author Contributions

The manuscript was written through contributions of all authors. All the authors have viewed and given approval to the final version.

Notes

The authors declare no competing financial interest.

■ ACKNOWLEDGMENTS

This work is financially supported by the National Basic Research Program of China (Grant No. 2011CB707603 and 2011CB707604) and the National Natural Science Foundation of China with Grant No. 51175281.

DOI: 10.1021/acs.jpcc.5b00047
J. Phys. Chem. C 2015, 119, 8329−8335

REFERENCES

(1) Branton, D.; Deamer, D. W.; Marziali, A.; Bayley, H.; Benner, S. A.; Butler, T.; Di Ventra, M.; Garaj, S.; Hibbs, A.; Huang, X.; et al. The Potential and Challenges of Nanopore Sequencing. *Nat. Biotechnol.* **2008**, *26*, 1146−1153.

(2) Schneider, G. F.; Dekker, C. DNA Sequencing with Nanopores. *Nat. Biotechnol.* **2012**, *30*, 326−328.

(3) Dekker, C. Solid-State Nanopores. *Nat. Nanotechnol.* **2007**, *2*, 209−215.

(4) Wanunu, M. Nanopores: A Journey towards DNA Sequencing. *Phys. Life Rev.* **2012**, *9*, 125−158.

(5) Zwolak, M.; Di Ventra, M. Colloquium: Physical Approaches to DNA Sequencing and Detection. *Rev. Mod. Phys.* **2008**, *80*, 141−165.

(6) Pennisi, E. Search for Pore-fection. *Science* **2012**, *336*, 534−537.

(7) Pennisi, E. DNA Sequencers Still Waiting for the Nanopore Revolution. *Science* **2014**, *343*, 829−830.

(8) Coulter, W. H. *Means for Counting Particles Suspended in a Fluid*. U.S. Patent No. 2,656,508, 1953.

(9) Firnkes, M.; Pedone, D.; Knezevic, J.; Doeblinger, M.; Rant, U. Electrically Facilitated Translocations of Proteins through Silicon Nitride Nanopores: Conjoint and Competitive Action of Diffusion, Electrophoresis, and Electroosmosis. *Nano Lett.* **2010**, *10*, 2162−2167.

(10) Slonkina, E.; Kolomeisky, A. B. Polymer Translocation through a Long Nanopore. *J. Chem. Phys.* **2003**, *118*, 7112−7118.

(11) Venta, K. E.; Zanjan, M. B.; Ye, X.; Danda, G.; Murray, C. B.; Lukes, J. R.; Drndic, M. Gold Nanorod Translocations and Charge Measurement through Solid-State Nanopores. *Nano Lett.* **2014**, *14*, 5358−5364.

(12) Tsutsui, M.; Maeda, Y.; He, Y.; Hongo, S.; Ryuzaki, S.; Kawano, S.; Kawai, T.; Taniguchi, M. Trapping and Identifying Single-Nanoparticles Using a Low-Aspect-Ratio Nanopore. *Appl. Phys. Lett.* **2013**, *103*, 013108.

(13) Arjmandi, N.; Van Roy, W.; Lagae, L.; Borghs, G. Measuring the Electric Charge and Zeta Potential of Nanometer-Sized Objects Using Pyramidal-Shaped Nanopores. *Anal. Chem.* **2012**, *84*, 8490−8496.

(14) Tsutsui, M.; Hongo, S.; He, Y.; Taniguchi, M.; Gemma, N.; Kawai, T. Single-Nanoparticle Detection Using a Low-Aspect-Ratio Pore. *ACS Nano* **2012**, *6*, 3499−3505.

(15) Kozak, D.; Anderson, W.; Vogel, R.; Chen, S.; Antaw, F.; Trau, M. Simultaneous Size and Zeta-Potential Measurements of Individual Nanoparticles in Dispersion Using Size-Tunable Pore Sensors. *ACS Nano* **2012**, *6*, 6990−6997.

(16) Deblois, R. W.; Bean, C. P.; Wesley, R. K. Electrokinetic Measurements with Submicron Particles and Pores by the Resistive Pulse Technique. *J. Colloid Interface Sci.* **1977**, *61*, 323−335.

(17) DeBlois, R. W.; Wesley, R. K. Sizes and Concentrations of Several Type C Oncornaviruses and Bacteriophage T2 by the Resistive-Pulse Technique. *J. Virol.* **1977**, *23*, 227−233.

(18) Prabhu, A. S.; Jubery, T. Z. N.; Freedman, K. J.; Mulero, R.; Dutta, P.; Kim, M. J. Chemically Modified Solid State Nanopores for High Throughput Nanoparticle Separation. *J. Phys.-Condens. Mater.* **2010**, *22*, 454107.

(19) Astier, Y.; Datas, L.; Carney, R.; Stellacci, F.; Gentile, F.; DiFabrizio, E. Artificial Surface-Modified Si_3N_4 Nanopores for Single Surface-Modified Gold Nanoparticle Scanning. *Small* **2011**, *7*, 455−459.

(20) Lan, W.-J.; Holden, D. A.; Zhang, B.; White, H. S. Nanoparticle Transport in Conical-Shaped Nanopores. *Anal. Chem.* **2011**, *83*, 3840−3847.

(21) Bacri, L.; Oukhaled, A. G.; Schiedt, B.; Patriarche, G.; Bourhis, E.; Gierak, J.; Pelta, J.; Auvray, L. Dynamics of Colloids in Single Solid-State Nanopores. *J. Phys. Chem. B* **2011**, *115*, 2890−2898.

(22) Davenport, M.; Healy, K.; Pevarnik, M.; Teslich, N.; Cabrini, S.; Morrison, A. P.; Siwy, Z. S.; Letant, S. E. The Role of Pore Geometry in Single Nanoparticle Detection. *ACS Nano* **2012**, *6*, 8366−8380.

(23) Aksimentiev, A.; Heng, J. B.; Timp, G.; Schulten, K. Microscopic Kinetics of DNA Translocation through Synthetic Nanopores. *Biophys. J.* **2004**, *87*, 2086−2097.

(24) Heng, J. B.; Ho, C.; Kim, T.; Timp, R.; Aksimentiev, A.; Grinkova, Y. V.; Sligar, S.; Schulten, K.; Timp, G. Sizing DNA Using a Nanometer-Diameter Pore. *Biophys. J.* **2004**, *87*, 2905−2911.

(25) Chang, H.; Kosari, F.; Andreadakis, G.; Alam, M. A.; Vasmatzis, G.; Bashir, R. DNA-Mediated Fluctuations in Ionic Current through Silicon Oxide Nanopore Channels. *Nano Lett.* **2004**, *4*, 1551−1556.

(26) Fan, R.; Karnik, R.; Yue, M.; Li, D. Y.; Majumdar, A.; Yang, P. D. DNA Translocation in Inorganic Nanotubes. *Nano Lett.* **2005**, *5*, 1633−1637.

(27) Chang, H.; Venkatesan, B. M.; Iqbal, S. M.; Andreadakis, G.; Kosari, F.; Vasmatzis, G.; Peroulis, D.; Bashir, R. DNA Counterion Current and Saturation Examined by a MEMS-Based Solid State Nanopore Sensor. *Biomed. Microdevices* **2006**, *8*, 263−269.

(28) Smeets, R. M. M.; Keyser, U. F.; Krapf, D.; Wu, M. Y.; Dekker, N. H.; Dekker, C. Salt Dependence of Ion Transport and DNA Translocation through Solid-State Nanopores. *Nano Lett.* **2006**, *6*, 89−95.

(29) Kowalczyk, S. W.; Dekker, C. Measurement of the Docking Time of a DNA Molecule onto a Solid-State Nanopore. *Nano Lett.* **2012**, *12*, 4159−4163.

(30) Goyal, G.; Freedman, K. J.; Kim, M. J. Gold Nanoparticle Translocation Dynamics and Electrical Detection of Single Particle Diffusion Using Solid-State Nanopores. *Anal. Chem.* **2013**, *85*, 8180−8187.

(31) Menestrina, J.; Yang, C.; Schiel, M.; Vlassiouk, I.; Siwy, Z. S. Charged Particles Modulate Local Ionic Concentrations and Cause Formation of Positive Peaks in Resistive-Pulse-Based Detection. *J. Phys. Chem. C* **2014**, *118*, 2391−2398.

(32) Innes, L. M.; Chen, C. H.; Schiel, M.; Pevarnik, M.; Haurais, F.; Toimil-Molares, M. E.; Vlassiouk, I.; Theogarajan, L.; Siwy, Z. S. Velocity Profiles in Pores with Undulating Opening Diameter and Their Importance for Resistive-Pulse Experiments. *Anal. Chem.* **2014**, *86*, 10445−10453.

(33) Lan, W.-J.; Kubeil, C.; Xiong, J.-W.; Bund, A.; White, H. S. Effect of Surface Charge on the Resistive Pulse Waveshape during Particle Translocation through Glass Nanopores. *J. Phys. Chem. C* **2014**, *118*, 2726−2734.

(34) Cabello-Aguilar, S.; Abou Chaaya, A.; Picaud, F.; Bechelany, M.; Pochat-Bohatier, C.; Yesylevskyy, S.; Kraszewski, S.; Bechelany, M. C.; Rossignol, F.; Balanzat, E.; et al. Experimental and Simulation Studies of Unusual Current Blockade Induced by Translocation of Small Oxidized PEG through a Single Nanopore. *Phys. Chem. Chem. Phys.* **2014**, *16*, 17883−17892.

(35) Liu, H.; Qian, S.; Bau, H. H. The Effect of Translocating Cylindrical Particles on the Ionic Current through a Nanopore. *Biophys. J.* **2007**, *92*, 1164−1177.

(36) Ai, Y.; Qian, S. Direct Numerical Simulation of Electrokinetic Translocation of a Cylindrical Particle through a Nanopore Using a Poisson−Boltzmann Approach. *Electrophoresis* **2011**, *32*, 996−1005.

(37) Wang, J.; Ma, J.; Ni, Z.; Zhang, L.; Hu, G. Effects of Access Resistance on the Resistive-Pulse Caused by Translocating of a Nanoparticle through a Nanopore. *RSC Adv.* **2014**, *4*, 7601−7610.

(38) Cabello-Aguilar, S.; Chaaya, A. A.; Bechelany, M.; Pochat-Bohatier, C.; Balanzat, E.; Janot, J. M.; Miele, P.; Balme, S. Dynamics of Polymer Nanoparticles through a Single Artificial Nanopore with a High-Aspect-Ratio. *Soft Matter* **2014**, *10*, 8413−8419.

(39) Lan, W. J.; Holden, D. A.; White, H. S. Pressure-Dependent Ion Current Rectification in Conical-Shaped Glass Nanopores. *J. Am. Chem. Soc.* **2011**, *133*, 13300−13303.

(40) Rayleigh, L. On the Influence of Obstacles Arranged in Rectangular Order upon the Properties of a Medium. *Philos. Mag.* **1892**, *34*, 481−502.

(41) Hall, J. E. Access Resistance of a Small Circular Pore. *J. Gen. Physiol.* **1975**, *66*, 531−532.

DOI: 10.1021/acs.jpcc.5b00047
J. Phys. Chem. C 2015, 119, 8329−8335